Jpn. J. Appl. Phys. Vol. 42 (2003) pp. 6303–6307
Part 1, No. 10, October 2003

Local Structural Properties in the Terahertz Semiconductor $Zn_{1-x}Cd_xTe$

Sang-Wook HAN

Chemical Sciences Division, Lawrence Berkeley, National Laboratory, Berkeley, California 94720, USA

(Received January 27, 2003; revised May 13, 2003; accepted June 20, 2003; published October 9, 2003)

Local structural properties of wide-band-gap semiconductors, $Zn_{1-x}Cd_xTe$ (ZCT) crystals ($x = 0$–0.25), were studied using X-ray absorption fine structure (XAFS) measurements at the Te L_1- and Zn K-edges. A previous study by Liu *et al.*[1] reported that ZCT emits or absorbs terahertz (THz) signals with a best efficiency when $x \simeq 0.05$. The XAFS studies show that the disorder and the bond length of Te–Zn pairs have maximum values at about $x = 0.05$. We discuss that these structural transitions are relevant to the efficiency of THz emission and absorption in ZCT crystals. We also find that the distance of Te–Cd pairs is at least ~0.2 Å longer than that of Te–Zn pairs and that Cd doping causes disorder/distortion in both Te and Zn sites in the crystals. [DOI: 10.1143/JJAP.42.6303]

KEYWORDS: ZnCdTe, terahertz, local structure, disorder, XAFS, semiconductor

1. Introduction

$Zn_{1-x}Cd_xTe$ (ZCT) with a small amount of Cd doping (including no doping) is a well-known light p-type semiconductor with a wide energy band gap. Oriented ($\langle 110 \rangle$) ZCT crystals have attracted considerable interest for their practical applications in detectors or as sources of terahertz (THz) pulses.[1–6] Liu *et al.*[1] have observed that the efficiency of ZCT crystals in emitting and absorbing THz pulses increases by ~16% for absorption and by ~4% for emission when $x = 0.05$, compared to $x = 0.0$, but then decreases at composition ratios of $x > 0.05$. They showed that the efficiency of ZnTe for THz emission is about 11 times greater than that of CdTe. The efficiency difference between ZnTe and CdTe can be understood in terms of the energy band gap of the crystals.[7] However, it is not clear how a small amount of Cd doping ($x \simeq 0.05$) enhances these efficiencies.

As a Cd^{2+} ($4d^{10}5s^0$) ion is doped in a Zn^{2+} ($3d^{10}4s^0$) site, the chemical difference of the ions likely does not contribute to a change of energy band structure because their chemical properties are quite similar. However, the difference in the atomic sizes between Zn and Cd could play a role in the efficiencies of the absorption or emission of THz signals. ZCT has a zinc-blende structure, i.e., Zn has 4 Te neighbors and Te has 4 Zn neighbors and the covalent radius of Zn is ~1.31 Å and that of Cd is ~1.48 Å. When Cd is doped in the Zn site, the structural properties would be changed because of the difference in atomic size possibly generating defects (disorder) in the crystal. There are a number of theoretical and experimental studies on the effect of defects in THz semiconductors, such as, GaAs,[8] N-doped Zn-based materials (ZnS, ZnSe, ZnTe),[9] Zn-based-zinc-blende-structured materials ($ZnSe_{1-x}Te_x$, $Zn_{1-x}Be_xSe$, $Zn_{1-x}Cd_xSe$),[10] ZnTe,[11,12] p-$Cd_{0.96}Zn_{0.04}Te$,[13] and others. We explore the possibility of structural changes in the ZCT crystals with X-ray absorption fine structure (XAFS) measurements. To our best knowledge, no study of local structural properties in ZCT crystals has yet been reported.

We investigate the environments of the Te and Zn atoms in $Zn_{1-x}Cd_xTe$ ($x = 0.0$, 0.05, 0.15, 0.25) with the XAFS spectroscopic technique. XAFS acts as a probe to detect partial pair distribution functions of atom pairs, so that the Zn/Cd atoms near a probe Te atom and Te atoms near a probe Zn atom can be effectively studied. The zinc sites near the Te atom are partially occupied by Cd atoms. From the probe Te atom, the Zn site, distorted by dopant Cd, can be studied while the bond length and disorder of the Zn–Te pairs, untouched by the Cd atoms, can be measured from the probe Zn atom.

In this paper, the sample preparation and XAFS measurements are described in §2 and the data analysis and results of the experiments are shown in §3. In §4, we discuss the results and summarize the main conclusions in §5.

2. Experimental Details

Single $Zn_{1-x}Cd_xTe$ ($x = 0.0$, 0.05, 0.15, 0.25) crystals were grown in a vertical Bridgeman furnace with advanced growth technology.[1] The single crystal ingot was ground in acetone and sieved with a 25 μm sieve. X-ray powder diffraction (XRD) measurements confirm that the crystal structure is zinc blende without an extra phase and the lattice constant of ZnTe is 6.092 ± 0.003 Å at room temperature. The sieved powders were uniformly spread on Scotch tape with a brush and the tape was layered to achieve an edge-step of total X-ray absorption (μx) of about one. Transmission XAFS measurements were performed at beamline 3C1 of the Pohang Light Source. Incident X-ray energy was tuned with a Si(111) double monochromator.

Figure 1 shows the total XAFS measurements of

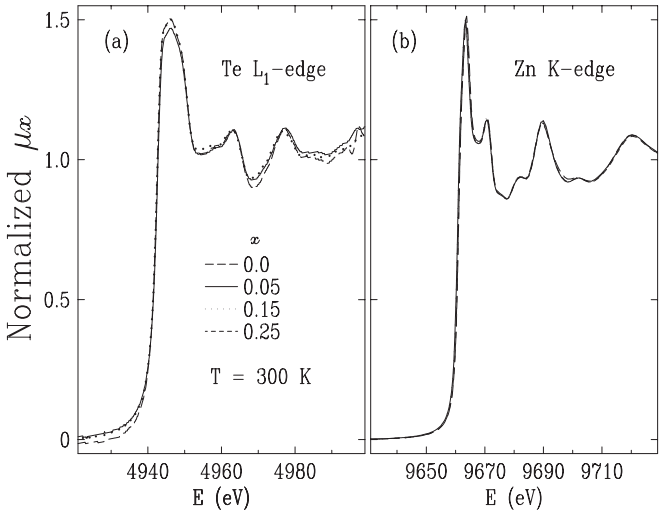

Fig. 1. Normalized total X-ray absorption from $Zn_{1-x}Cd_xTe$ as a function of incident X-ray energy at (a) Te L_1-edge and (b) Zn K-edge.

$Zn_{1-x}Cd_xTe$ at different composition ratios of x at the (a) Te L_1-edge and (b) Zn K-edge. The pre-edge of the data was removed and the data were normalized to an edge-step of 1. Observations of the Te edges show a small but significant difference in edge height as a function of the Zn/Cd composition ratio. This change in the absorption edge can be explained by changes in the energy band structure. Since Zn and Cd have similar chemical properties, the difference in the edge height could be attributed to structural changes in the crystals resulting from Cd doping. The structural change can be more clearly seen from the analysis of extended X-ray absorption fine structure (EXAFS). The oscillations, EXAFS, at the post-edge are due to interaction between the outgoing electrons from a probe atom and the back scattered electrons from the neighbor atoms.[14–16] From analyzing EXAFS, relative distances from the probe atom, coordination numbers, atomic species and disorder factors of the neighbor atoms can be obtained, as shown in eq. (1).

3. Data Analysis and Results

The X-ray absorption coefficient above the edge can be described by $\mu(k) = \mu_0(k)(1 + \chi(k))$, where $k = \sqrt{2m(E - E_f)}/\hbar$ is the photoelectron wave number relative to the Fermi wave number. For K-edges ($1s$), the EXAFS modulation can be written within the harmonic approximation for lattice vibrations[14–16] as,

$$\chi(k) = -\sum_j 3(\hat{\epsilon}\cdot\hat{r}_j)^2 \frac{S_0^2 N_j F_j(\pi,k,r_j)}{kr_j^2} e^{-2k^2\sigma_j^2} e^{-2r_j/\lambda(k)} \times \sin(2kr_j + \phi(k,r_j)), \quad (1)$$

where $\hat{\epsilon}$ is the electric field direction of the incident X-rays, N_j is the coordination number of the jth shell of atoms, S_0^2 accounts for the change of the passive electron wave functions in the presence of a core hole and multi-electron excitations, F_j is an effective curved wave backscattering amplitude, r_j is the effective interatomic distance, σ_j^2 is the mean-squared relative displacement in the effective interatomic distance, λ is an effective mean-free path which includes the finite lifetime of the core hole, ϕ is an overall scattering phase shift from the probe and jth backscattering atoms. Multiple scattering paths are included in the data analysis and the polarization effect of the X-ray was not applied for the data analysis because the measurements were made on powder.

In order to analyze the measured EXAFS data, we used the UWXAFS package.[17] First, $\chi(k)$ was extracted by subtraction of the atomic background, $\mu_0(k)$, from the raw data $\mu(k)$. Only the EXAFS data in the k-range of 2.5–9.0 Å^{-1} for the Te L_1-edge and 3.0–12.0 Å^{-1} for the Zn K-edge were used for further analysis. Choosing the lower cut-off k point anywhere in the range 2.5–3.5 Å^{-1} produces insignificant variation of the fit parameters. Additional details of the EXAFS analysis and the determination of a goodness of fit have been given elsewhere.[18]

Figure 2(a) shows the magnitude of the Fourier transformed EXAFS with weight k measured at the L_1-edge for different composition ratios of Cd. The abscissa $\tilde{r}$ is about 0.4 Å shorter than the true distances from the probe Te atom because the phase shift correction was not applied. The first shell corresponds to 4 Zn/Cd atoms, and the second shell comes from 12 Te atoms. The data were fit with a EXAFS theory in FEFF7.[19] The total EXAFS was obtained by the summation of EXAFS of each atom with a weight: $\chi(k) = \chi_{Te} + \chi_{Zn} \times (1 - x) + \chi_{Cd} \times (x)$, where x is the ratio of the Cd composition, assuming that the Cd atom is randomly distributed over the Zn site. The EXAFS data and a best fit for the specific crystal of $Zn_{0.95}Cd_{0.05}Te$ are shown in Fig. 2(b). The results of the fit are summarized in Table I. A small r-factor indicates that the fit is very good. However, a large value of the χ_ν^2 which is expected to be 1.0 implies that systematic uncertainty is about 5 times larger than what we count in the fit. S_0^2 of ~1.0 indicates that the contribution of the core hole and multi-electron excitations to the photoelectron wave is negligible. There is linear correlation between S_0^2 and the coordination numbers [see eq. (1)]. However, we can still estimate that the atomic sites (Te and Zn) near the Te atom are fully occupied within an uncertainty of 20%, by varying the coordination numbers in the fit because S_0^2 is independent of the chemical environment. All four sets of data at different composition ratios of x were analyzed using the same procedure.

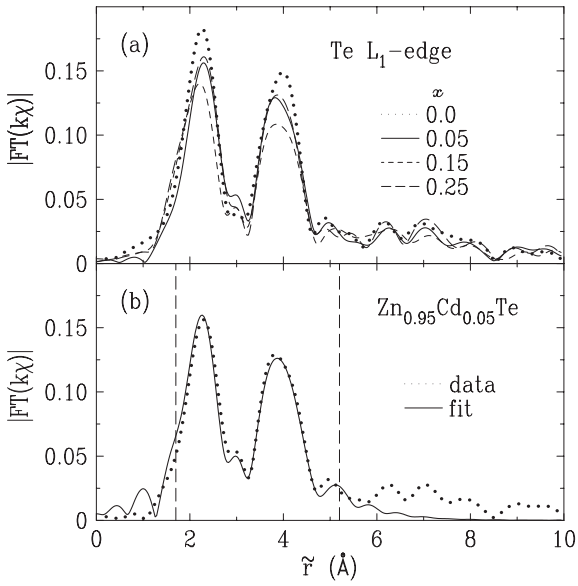

Fig. 2. (a) Magnitude of Fourier transformed EXAFS data measured at the Te L_1-edge in $Zn_{1-x}Cd_xTe$ for different Cd compositions. (b) EXAFS data (dotted line) for $Zn_{0.95}Cd_{0.05}Te$ and a fit (solid line). The fit region is indicated by vertical dashed lines in (b).

Table I. Results of non-linear least squares fits of $Zn_{0.95}Cd_{0.05}Te$ are shown. Reduced-χ^2 (χ_ν^2) is the total χ^2 divided by the fit freedom (ν) which is the total number of independent data points (N_I) minus the number of variables in the fits. N_I is determined by Stern's rule;[17,19] $(2\Delta k\Delta r/\pi + 2)$ where Δk is the region of k in which the data were used for Fourier transform into r-space and Δr is the fit region.

Edge	χ_ν^2	r-factor	N_I	ν	S_0^2
Te L_1	26.7	0.009	16	8	1.0 (0.1)
Zn K	49.2	0.002	21	14	0.91 (0.05)

Figure 3(a) shows the bond lengths of Te–Zn and Te–Te pairs which correspond to the first and the second peaks, respectively, in Fig. 2. The bond length of the Te–Zn pairs increases from $x = 0$ to $x = 0.05$ but decreases slightly at

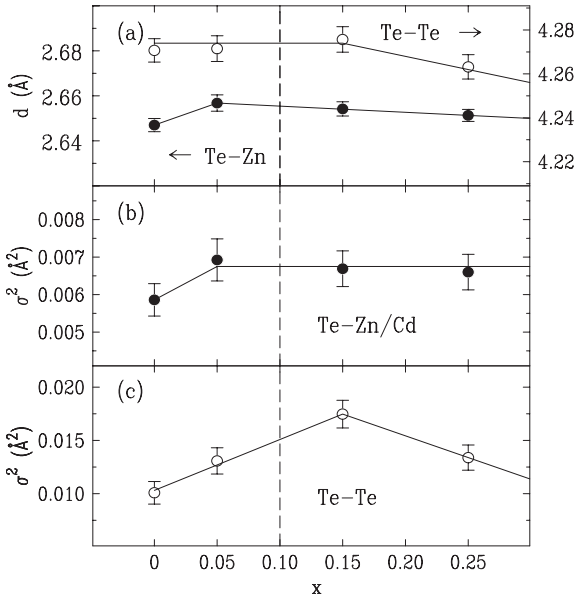

Fig. 3. Bond lengths of the Te–Te pairs (open circles) and the Te–Zn pairs (closed circles), as a function of the Cd composition, determined from the Te L_1-edge are shown in (a). Please, be aware of the scales: left is for the Te–Zn pairs and right is for the Te–Te pairs. The solid lines are a guide to the eye. Debye–Waller factors (σ^2) for (b) Te–Zn/Cd pairs and (c) Te–Te pairs.

Table II. Bond length of Te–Cd pairs.

x	0.05	0.15	0.25
d (Å)	2.95 (0.180)	2.895 (0.058)	3.036 (0.072)

higher Cd compositions while the bond length of Te–Te pairs remains constant for $x \leq 0.15$ and decreases for $x \geq 0.15$. The distance of Te–Cd pairs is ~0.2–0.3 Å longer than that of Te–Zn pairs. The difference in the distance is comparable to the radius difference of the Zn and Cd atoms. The distances of Te–Cd pairs at the different composition ratios of Cd are summarized in Table II. The Debye–Waller factors (σ^2, including thermal vibration and static disorder) of (b) Te–Zn/Cd pairs and (c) Te–Te pairs are shown in Fig. 3. The σ^2 of the Te–Zn/Cd pairs (Te–Te pairs) increases for small amounts of Cd-doping, $x \leq 0.05$ (0.15). For $x > 0.05$, the disorder of the Te–Zn/Cd pairs is roughly constant while the disorder of Te–Te pairs decreases for $x > 0.15$. In the fit, the distances of Te–Zn and Te–Cd pairs were independently varying while the σ^2s of the Te–Zn and Te–Cd pairs were fit with the same variable because the σ^2s of the Te–Zn and Te–Cd pairs are highly correlated in the fit.

From the Zn K-edge measurements, we can cross-check the results obtained at the Te L_1-edge. Moreover, the Zn–Te pairs which are not affected by the Cd doping and the Zn–Zn/Cd pairs can be studied. Figure 4 shows (a) the magnitude of the Fourier transformed EXAFS data, as a function of the distance from the Zn probe atoms, for different composition ratios of Cd and (b) the EXAFS from $Zn_{0.95}Cd_{0.05}Te$ and a best fit. The results of the fit are summarized in Table I. From the analysis, a vacancy in the Te site is not observed with an uncertainty of about 20%. In the fit, the Zn–Cd distance (~4.5 Å) was varied using the Zn–Zn pair distance with addition of 0.2 Å because the bond lengths of Zn–Zn and Zn–

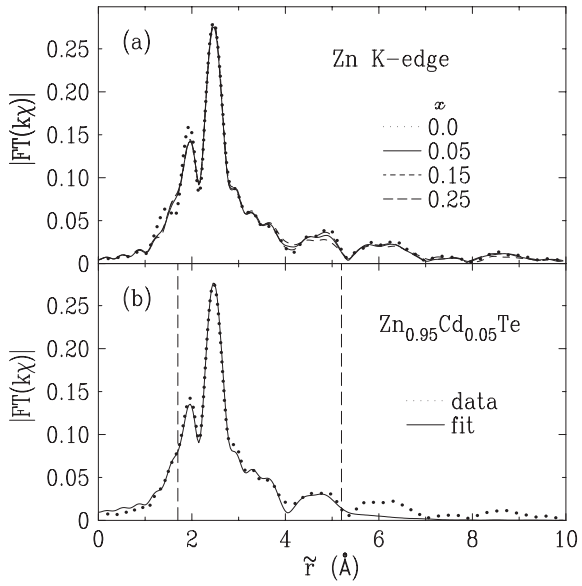

Fig. 4. (a) Magnitude of Fourier transformed EXAFS data measured at the Zn K-edge in $Zn_{1-x}Cd_xTe$. (b) EXAFS data (dotted line) for $Zn_{0.95}Cd_{0.05}Te$ and a fit (solid line). Vertical lines in (b) indicate the fit region.

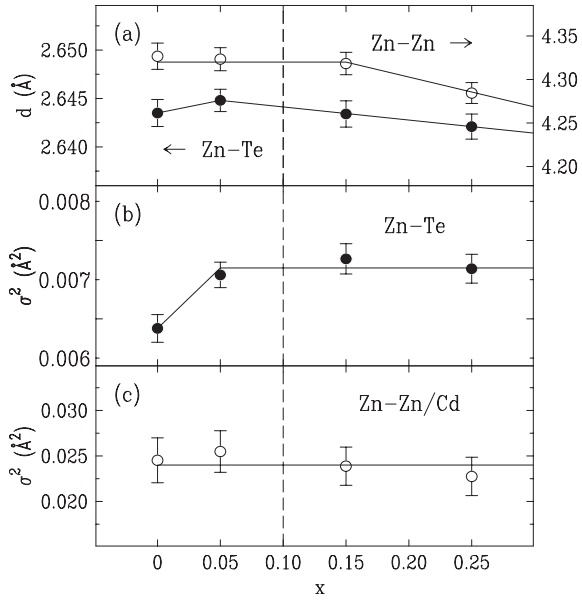

Fig. 5. (a) shows bond lengths of the Zn–Zn pairs (open circles) and the Zn–Te pairs (closed circles) as a function of the Cd composition determined from the Zn K-edge. Please, be aware of the scales: left is for Zn–Te pairs and right is for Zn–Zn pairs. The solid lines are a guide to the eye. σ^2s for (b) Zn–Te pairs and (c) Zn–Zn/Cd pairs.

Cd pairs are not distinguishable due to a high correlation between the distances and the σ^2s of the pairs. Figure 5(a) shows the bond lengths of the Zn–Te and Zn–Zn pairs. The distance of the Zn–Te pairs increases slightly for small amounts of Cd doping ($x \leq 0.05$) but decreases at higher Cd doping levels. The bond length of the Zn–Zn pairs does not change for $x \leq 0.15$ and decreases for $x > 0.15$. σ^2s are shown in Fig. 5(b) for the Zn–Te pairs and in (c) for the Zn–Zn/Cd pairs. At low levels of Cd doping ($x \leq 0.05$) the σ^2 of the Zn–Te pairs increases but then remains constant, within

uncertainty, at higher composition ratios of Cd. The disorder of the Zn–Zn/Cd pairs does not change until the Cd composition of 0.25, within uncertainty. The relatively large amount of disorder of the Zn–Zn/Cd pairs might be due to the thermal vibration of the pairs because the Zn atom is lighter than the Te atom.

From the comparison of Te–Zn/Cd [Fig. 3(b)] and Zn–Te [Fig. 5(b)], the disorders are not distinguishable within uncertainty. This implies that the Cd dopant affects the Te site as well as the Zn site. The bond length of the Te–Zn pairs measured at the Te L_1-edge is about 0.012 Å longer than that of Zn–Te measured at the Zn K-edge in all ZCT crystals with the exception of the ZnTe crystal [see Fig. 3(a) and Fig. 5(a)]. This strongly suggests that the doped Cd atom creates a distortion in the Zn site. Our observations show that the crystalline structure in ZnTe is more ordered than in the other ZCT crystals and that a small amount of Cd doping in the Zn site slightly distorts the crystal and increases disorder in all atomic sites.

4. Discussion

In the zinc-blende structure of ZCT, Te (Zn) has 4 Zn (Te) neighbors at about 2.65 Å and 12 Te (Zn) neighbors at about 4.27 Å. For small amounts of Cd doping ($x = 0.05$), the Te–Te (Zn–Zn) pairs have the same bond length while the Te–Zn pairs show substantial increases in the bond length and the disorder values compared with the ZnTe crystal. These observations suggest that at $x = 0.05$ the crystalline structure slightly expands along the direction of the Te–Zn bond and shrinks in the direction perpendicular to the bond. The expansion is expected to occur along the $\langle 111 \rangle$ direction because atoms are stacked with an *ABAB* pattern along the $\langle 111 \rangle$ direction in the zinc-blende structure, although we cannot disregard the possibility of an expansion in other directions. If the crystal is slightly elongated along the $\langle 111 \rangle$ direction and compressed in the direction perpendicular to $\langle 111 \rangle$, the average bond lengths of the Te–Te and Zn–Zn pairs can be expected to remain constant, but the σ^2s of the pairs will increase because the measured bond length of the Te–Te (Zn–Zn) pairs is averaged over 12 Te (Zn) neighbors which are located in all directions. These structural transitions agree with X-ray diffraction studies (XRD) by Han *et al.*[20] who observed an orthorhombic-like structure in ZnTe and a disordered-cubic structure in $Zn_{0.95}Cd_{0.05}Te$. With these results, we might conclude that the crystalline ZnTe does not have an exact cubic structure and a small amount of Cd dopant increases the cubic symmetry in the ZCT crystals.

It is known that optical rectification is maximized as optical waves propagate along the $\langle 110 \rangle$ direction in the ZCT crystal.[1] If a crystalline structure is orthorhombic with slightly different lattice constants, it can be expected that a twin-like structure might exist in the bulk. Our studies imply that a ZCT crystal with a more periodic atomic structure (cubic symmetry) has a better efficiency of both absorbing and emitting THz signals compared with Liu's studies.[1] In order to obtain a better efficiency of THz in an optically nonlinear material, a larger phase match (longer coherence length) between the optical-pump and THz pulses is an essential parameter. The phase matching condition for the optical rectification process for two waves with different frequencies in a collinear axis can be described as:[21] $\Delta k = k_{\mathrm{opt+THz}} - k_{\mathrm{opt}} - k_{\mathrm{THz}} = 0$, where k_{opt} and k_{THz} are the wave numbers of the optical and THz pulses, respectively, and $k_{\mathrm{opt+THz}}$ is the wave number of the two mixed pulses in a material. The coherence length is defined to be $\pi c/\Delta k$, where c is the speed of light in vacuum. Using the dispersion of the optical frequencies and the phase matching condition, the coherence length (l_c) is shown to be:

$$l_c = \frac{c f_{\mathrm{THz}}}{2\left| n_{\mathrm{opt}} - \lambda_{\mathrm{opt}} \left.\frac{dn_{\mathrm{opt}}}{d\lambda}\right|_{\lambda_{\mathrm{opt}}} - n_{\mathrm{THz}} \right|}, \tag{2}$$

where f_{THz} is the frequency in THz, n_{opt} and n_{THz} are the refractive indices of the optical and THz pulses, respectively. If Cd atoms were randomly spread on the exact Zn sites and no further structural changes were made, we would expect that l_c might be linearly decreased as a function of Cd composition due to the differences in the optical properties as well as the band gaps between ZnTe and CdTe crystals.[22] However, our results suggest that the effect of the structural change to the THz efficiency may not be negligible and that the magnitude of the optical dispersion $(dn_{\mathrm{opt}}/d\lambda)|_{\lambda_{\mathrm{opt}}}$ is smaller in a cubic than in an orthorhombic environment compared with eq. (2) because the dispersion relation of the optical wave has a negative value and the optical and THz refractive indices may not be changed much by this small amount of distortion.

Although we observe slight elongation in the Te–Zn bond length for $x \simeq 0.05$ compared to that in the ZnTe crystal, it is not clear whether the ZCT crystals follow Vegard's law because we could not ignore the possibility of shorter bond lengths of the Te–Te and Zn–Zn pairs in the direction perpendicular to the Te–Zn bond. Saito *et al.*[23] reported the observation that zinc-blende-structured crystals of $Zn_{1-x}Cr_xTe$ followed Vegard's law. Because the atomic radius of Cd is larger than that of Zn, we might expect that the distances of atomic pairs are continuously increased with the composition ratio of Cd. However, our observations do not follow this prediction well for the Cd doping range of 0–0.25. There could be several reasons why Vegard's law may not be obeyed in ZCT crystals; i) XAFS may not be sensitive enough to determine the small amount of volume expansion, ii) distortions/disorder compensate for the expansion, and iii) the Cd atoms do not occupy exact Zn sites. We could not determine the Cd behavior in the crystals accurately due to the limits in XAFS sensitivity.

5. Conclusions

We have studied the structural properties near the Te and Zn atoms in $Zn_{1-x}Cd_xTe$ crystals ($x = 0.0, 0.05, 0.15, 0.25$) with a local structural probe. Accompanying Cd doping, all atomic sites are slightly more disordered and the bond length of Te–Zn pairs is increased while the bond lengths of Te–Te and Zn–Zn pairs remain constant for $x \leq 0.05$. The expansion in the crystal due to the Cd doping occurs along the $\langle 111 \rangle$ direction and increases the cubic symmetry of the crystals. The bond length of Te–Cd pairs is slightly longer than that of Te–Zn pairs by about 0.2 Å which is comparable to the difference of the covalent-bond radii of Cd and Zn atoms. These changes (distortions and disorder) of the local structural properties in ZCT crystals due to the Cd doping

should be included in proper theoretical models for the efficiency of ZCT crystals. With our XAFS studies, we could not discern whether ZCT crystals follow Vegard's law with certainty.

Acknowledgements

The author (S.-W. Han) is pleased to acknowledge the support from J. M. Lee for the XAFS measurements at the beamline 3C1 of the Pohang Light Source (PLS) in Korea. The experiments at PLS were supported in part by MOST and POSCO.

1) K. Liu, H.-S. Kang, T.-K. Kim and X.-C. Zhang: Appl. Phys. Lett. **81** (2002) 4115.
2) Q. Wu and X.-C. Zhang: Appl. Phys. Lett. **71** (1997) 1285.
3) Q. Wu, M. Litz and X.-C. Zhang: Appl. Phys. Lett. **68** (1996) 2924.
4) A. Leitenstorfer, S. Hunsche, J. Shah and M. C. Nuss: Appl. Phys. Lett. **74** (1999) 1516.
5) G. Gallot, J. Zhang, R. W. McGowan, T.-I. Jeon and D. Grischkowsky: Appl. Phys. Lett. **74** (1999) 3450.
6) Z. Piao, M. Tani and K. Sakai: Jpn. J. Appl. Phys. **39** (2000) 96.
7) M. Schall and P. Uhd Jepsen: Appl. Phys. Lett. **77** (2000) 2801.
8) D. T. J. Hurle: J. Appl. Phys. **85** (1999) 6957.
9) C. H. Park and D. J. Chadi: Phys. Rev. Lett. **75** (1995) 1134.
10) M.-H. Tsai, F. C. Peiris, S. Lee and J. K. Furdyna: Phys. Rev. B **65** (2002) 235202.
11) C. B. Norris: J. Appl. Phys. **53** (1982) 5172.
12) J. A. García, A. Remón, V. Muñoz and R. Triboulet: Jpn. J. Appl. Phys. **38** (1999) 5123.
13) M. D. Kim, T. W. Kang, J. M. Kim, H. K. Kim, Y. T. Jeong and T. W. Kim: J. Appl. Phys. **73** (1993) 4077.
14) E. A. Stern: Phys. Rev. B **10** (1974) 3027.
15) J. J. Rehr and R. C. Albers: Phys. Rev. B **41** (1990) 8139.
16) J. J. Rehr, R. C. Albers and S. I. Zabinsky: Phys. Rev. Lett. **69** (1992) 3397.
17) E. A. Stern, M. Newville, B. Ravel, Y. Yacoby and D. Haskel: Physica B **208–209** (1995) 117.
18) S.-W. Han, E. A. Stern, D. Hankel and A. R. Moodenbaugh: Phys. Rev. B **66** (2002) 094101.
19) A. L. Ankudinov and J. J. Rehr: Phys. Rev. B **56** (1997) 1712.
20) S.-W. Han and H.-S. Kang: unpublished, high resolution X-ray diffraction measurements show that the (111) diffraction peak from ZnTe splits into triplets while a single broad peak is observed from $Zn_{0.95}Cd_{0.05}Te$.
21) A. Nahata, A. S. Weling and T. F. Heinz: Appl. Phys. Lett. **69** (1996) 2321.
22) S. H. Wemple and M. diDomenico: *Advances in Materials and Device Research*, ed. Wolfe (Academic Press, New York, 1972) Vol. 3.
23) H. Saito, V. Zayets, S. Yamagata and K. Ando: Phys. Rev. B **66** (2002) 81201.